# Development of a 56 GHz ECH system for deuterium plasma experiments of a low magnetic field in LHD

# Development of 56 GHz ECH system for deuterium plasma experiment of a low magnetic field in LHD

R. Yanai[a,*], T. Ii Tsujimura[a], S. Kubo[a], Y. Yoshimura[a], T. Takeuchi[a], S. Ito[a], Y. Mizuno[a], M. Nishiura[a,b], H. Igami[a], N. Kenmochi[a], H. Takahashi[a,c], T. Shimozuma[a], M. Osakabe[a,c], T. Morisaki[a,c]

[a] *National Institute for Fusion Science, 322-6 Toki, Gifu 509-5292, Japan*
[b] *Graduate School of Frontier Sciences, The University of Tokyo, 5-1-5 Kashiwanoha, Kashiwa, Chiba, 277-8561 Japan*
[c] *Department of Fusion Science, The Graduate University for Advanced Studies, SOKENDAI, Toki, Gifu 509-5292, Japan*

**Abstract**

We have completed establishing the 56 GHz electron cyclotron heating (ECH) system with a new gyrotron to realize high $\beta$ plasma experiments with pure deuterium gas in the Large Helical Device (LHD). This new ECH system made it possible to conduct the relatively low magnetic field experiment around 1 T with pure deuterium gas because tangential neutral beam injection (NBI) systems of deuterium beams did not have enough power to initiate plasma in the LHD. We succeeded in initiating and sustaining pure deuterium plasma in the magnetic field of 1 T by using the 56 GHz ECH system and the deuterium NBI (D-NBI). This new ECH system contributed to expanding the new experiment regime in the LHD.

*Keywords:* ECH, LHD, plasma startup

## 1. Introduction

ECH is an essential auxiliary heating method for electron heating and current drive [1]. The characteristic of ECH of the local heating with high power density is important for plasma initiation of helical devices and for assisting inductive plasma startup in tokamak devices. ECH is expected to have an important role in plasma startup in ITER [2, 3].

The LHD is a heliotron type device whose nominal major radius and minor radius are 3.9 m and 0.6 m, respectively, with the toroidal periodicity of 10 [4, 5]. The LHD is equipped with ECH systems of 77 GHz and 154 GHz [6, 7] and three negative ion-based NBI systems (#1, #2, and #3) injecting neutral beams tangentially and two positive ion-based NBI systems (#4 and #5) injecting neutral

*Corresponding author
*Email address:* yanai@nifs.ac.jp (R. Yanai)

beams perpendicularly [8]. The deuterium plasma operation started from the 18th experimental campaign in 2017 to investigate the isotope effect on plasma parameters and characteristics in the LHD. The higher ion temperature and the better thermal confinement were found in the deuterium plasma compared with the hydrogen plasma in the LHD [9]. High $\beta$ plasma experiment relevant to nuclear fusion reactors is one of the most important research themes of the LHD [10]. Therefore, investigating the isotope effect of high $\beta$ plasma is a significant topic. The past high $\beta$ plasma experiment in the LHD used NBI plasma startup [11] since the 77 GHz or 154 GHz ECH could not initiate the plasma due to the relatively low magnetic field of about 1 T or less. Unfortunately, the tangential D-NBIs could not startup plasma because the tangential NBI systems were optimized for a hydrogen beam and the power of the tangential NBIs decreased [12]. The third harmonic extraordinary (X3) mode heating might be an option for plasma startup in the relatively low magnetic field condition but the attempts were failed in the LHD[13] or JT-60U[14] probably because plasma initiation using the X3 mode waves requires much stronger electric field than the fundamental or the second harmonic extraordinary (X2) mode waves[15]. For this reason, we installed a new 56 GHz gyrotron and established a new ECH system to realize pure deuterium plasma experiments with the relatively low magnetic field in the LHD.

The details of the new 56 GHz ECH system are introduced in section 2. The experimental results of plasma startup using the new ECH system are described in section 3. This paper is summarized in section 4.

## 2. 56 GHz ECH system

### *2.1.* 56 GHz *gyrotron oscillator system*

We installed the new gyrotron made by GYCOM as a 56 GHz high power oscillator. This gyrotron is a diode type with the collector potential depression. The parameters of the gyrotron in the factory test are summarized in Table. 1. In this test, the cathode voltage to ground $V_C$ was $-44$ kV and the body voltage to ground $V_B$ corresponding to the depression voltage $V_{dep}$ was 22 kV. Thus, the acceleration voltage $V_{acc}$ was 66 kV. We use two types of high voltage power supply systems to operate the gyrotron in our facility. A power supply system whose rated voltage and current in short time operation are 65 kV and 126 A, respectively, is used to apply $V_C$. The other system whose rated voltage and current are 30 kV and 200 mA, respectively, is used to apply $V_B$. The maximum output power measured in our facility reached around 490 kW when $V_{acc}$ was 69 kV, $V_{dep}$ was 21 kV, and the beam current was 21 A. Here, $V_C$ was $-48$ kV and $V_B$ was 21 kV. The estimated efficiency was more than 40 %. The microwave beam is output from the gyrotron as $TEM_{00}$ mode and the beam shape is formed by the matching optics unit (MOU) consisting of two mirrors to be coupled to the circular corrugated waveguide as $HE_{11}$ mode.

Table 1: Factory test results of 56 GHz gyrotron.

| | |
|---|---|
| Frequency | 56.05 GHz |
| Operating mode | $TE_{8,3}$ |
| RF power | 442 kW |
| Pulse duration of RF power | 1 s |
| Acceleration voltage | 66 kV |
| Depression voltage | 22 kV |
| Beam current | 22.5 A |
| Content of Gaussian beam | 97 % |

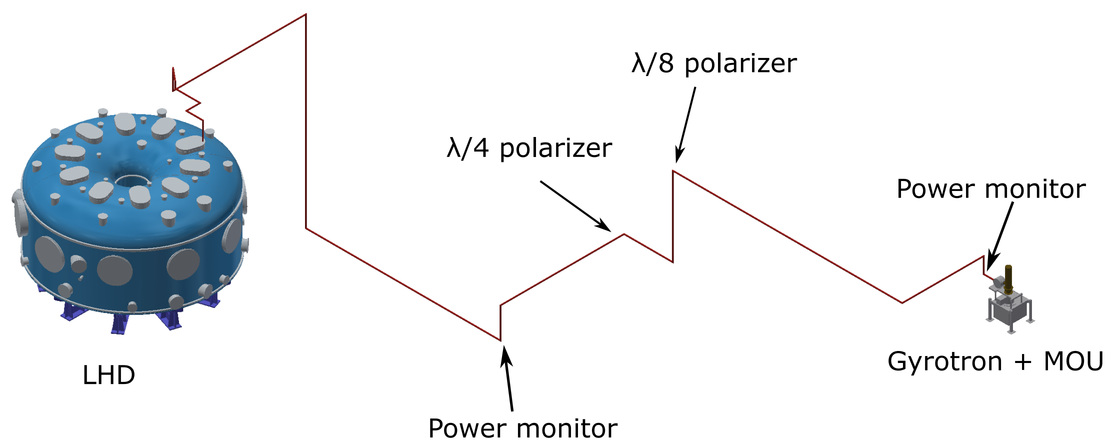


Fig. 1: Schematic view of transmission line of the 56 GHz ECH system.

### *2.2. ECH transmission line*

The microwave beam coupled to the circular corrugated waveguide is transmitted to the LHD. The circular corrugated waveguide whose inner diameter is 88.9 mm and whose corrugation pitch, width, and depth are 0.8 mm, 0.6 mm, and 0.6 mm, respectively, is used in the transmission line. Figure 1 indicates a schematic view of the transmission line from the gyrotron to the LHD. The transmission line of the 56 GHz ECH has 17 miterbends and the total length is over 100 m. Two of the miterbends are equipped with a directional coupler to monitor an RF signal. These power monitors are set at the miterbend nearest to the gyrotron and at the second miterbend after the $\lambda/4$ polarizer. The transmission line is evacuated and kept at less than 0.3 Pa to prevent arc discharge during transmitting the microwave beam. A sapphire vacuum window is attached to insulate the vacuum of the transmission line from that of the LHD. We assume that the transmitted power is 80 % of the gyrotron output power. We confirmed that the transmitted microwave beam kept a Gaussian-like profile near the LHD.

Each ECH transmission line of the LHD has a pair of polarizer mirrors of $\lambda/8$ and $\lambda/4$ at miterbends to set the arbitrary polarization direction $\alpha$ and ellipticity $\beta$ by changing the rotation angles of each polarizer mirrors [16]. Here, $\lambda$ is the wavelength of the transmitted microwave. The polarizer mirrors designed for 56 GHz microwaves are also installed in the 56 GHz ECH transmission line. Figure 2 indicates the polarization state of $\alpha$ and $\beta$ calculated from the rotation angle of the $\lambda/8$ polarizer $\Phi_{\lambda/8}$ and that of the $\lambda/4$ polarizer $\Phi_{\lambda/4}$, by changing $\Phi_{\lambda/8}$ and $\Phi_{\lambda/4}$, the microwave polarization can be controlled in the range of $-90^\circ \leq \alpha \leq 90^\circ$ and $-45^\circ \leq \beta \leq 45^\circ$. Figure 3 shows the comparison of the $\alpha$ dependence between the calculated and the experimental results of the detected RF power at the power monitor after the polarizers. The experimental results agreed reasonably well with those of the calculation.

### *2.3. System of antenna mirrors for* 56 GHz *microwave beam*

We designed and fabricated new antenna mirrors to complete plasma initiation by using the 56 GHz ECH and installed the mirrors in the LHD. Figure 4 shows the schematic view of the antenna mirrors and the shape of the propagating microwave beam after the transmission line. Here, we use a Cartesian coordinate $(R, T, Z)$ to determine the position to inject the ECH, where the $RT$-plane ($Z = 0$) is the equatorial plane of the LHD and the $RZ$-plane ($T = 0$) is the vertically elongated poloidal cross section and the $TZ$-plane ($R = 0$) is orthogonal to the other planes and includes the torus center of the LHD. The system of antennas to inject the EC beam consists of four mirrors. The first one is an aluminum flat mirror. The second and the third ones are aluminum concave mirrors. The final one is a stainless steel flat mirror. We adopted stainless steel to prevent the final mirror from being damaged by plasma because it directly faces plasma in the close position. This mirror can move around one axis. We can control the beam direction mainly in the radial direction from $R = 3.4\,\mathrm{m}$ to $R = 3.9\,\mathrm{m}$ on the equatorial plane by changing the reflection angle at the final mirror and the beam can be injected into the region of the normalized minor radius $\rho < 0.6$ in the standard magnetic configuration of the LHD, in which the magnetic axis position $R_{ax}$ is 3.6 m and the magnetic field at the magnetic axis $B_t$ is 1 T. All antenna mirrors are not cooled because of the relatively low power and the short pulse length of the 56 GHz ECH. Figure 5 indicates the spatial evolution of the elliptic Gaussian beam width $w_x$ and $w_y$ along the beam propagating direction and $w_x$ becomes the semi-minor axis and $w_y$ becomes the semi-major axis around an EC resonant position. Hence, the circular Gaussian beam output from the waveguide is changed to the elliptic Gaussian beam through the antenna mirrors and propagates toward the EC resonance. We designed the mirrors to shape the elliptical Gaussian beam to gain the beam cross-section as small as possible in the limited space of installing the mirrors. The power flux of the center of the Gaussian beam is expressed as $p_0 = 2P_{\mathrm{ECH}}/\pi w_x w_y$, where $P_{\mathrm{ECH}}$ is the injected power of ECH into plasma and is estimated at 80 % of the gyrotron output power. The angle between the semi-major axis of the elliptic Gaussian beam and the toroidal direction at $(R, T, Z) = (3.55\,\mathrm{m}, 0\,\mathrm{m}, 0\,\mathrm{m})$ is

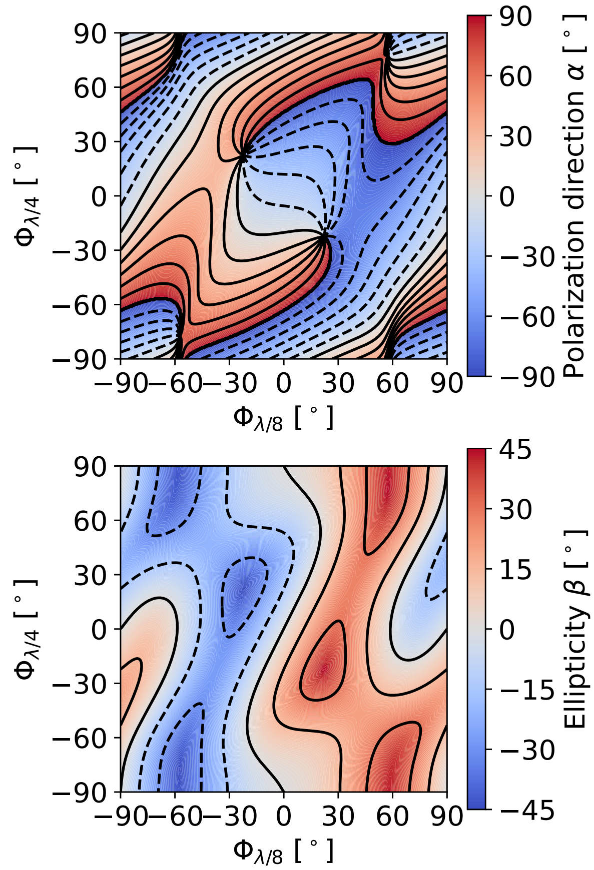


Fig. 2: Relations between the polarization state $(\alpha, \beta)$ and the polarizer angles of $\Phi_{\lambda/8}$ and $\Phi_{\lambda/4}$ of the 56 GHz microwave beam injected into $(R, T, Z) = (3.55\,\mathrm{m}, 0\,\mathrm{m}, 0\,\mathrm{m})$ in the LHD. The definition of $(R, T, Z)$ is described in subsection 2.3.

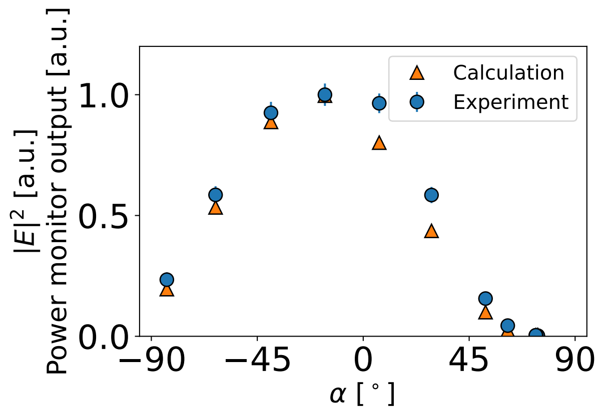


Fig. 3: Comparison of the dependence on $\alpha$ between (orange triangles) the calculated squared electric field component coupled to the power monitor $|E|^2$ and (blue circles) the power monitor output measured by a diode detector. The power monitor outputs were normalized by the maximum output at $\alpha \approx -16°$. The values of $|\beta|$ were less than 2°.

roughly 10°. The power flux and the power divided by the volume inside of the heated magnetic flux surface $p_V = P_{ECH}/V$ can be important parameters for plasma initiation, where $V$ is the volume inside of the heated magnetic flux surface. The past experimental data using the second harmonic EC resonance with the 77 GHz ECH revealed that $p_0 \geq 94\,\mathrm{MW/m^2}$ and $p_V \geq 48\,\mathrm{kW/m^3}$, when $P_{\mathrm{ECH}}$ was 110 kW in the polarization state of $(\alpha, \beta) \approx (-43°, -10°)$ and $V$ inside $\rho = 0.3$ was approximately $2.3\,\mathrm{m^3}$, were sufficient to initiate plasma in the LHD. We designed the antenna system to make $p_0$ and $p_V$ higher than the values. When $P_{\mathrm{ECH}}$ is 390 kW and the EC beam is injected into the direction of $(R, T, Z) = (3.55\,\mathrm{m}, 0\,\mathrm{m}, 0\,\mathrm{m})$ in the standard magnetic configuration of $R_{ax} = 3.6\,\mathrm{m}$ and $B_t = 1\,\mathrm{T}$, $w_x$ and $w_y$ are 31.8 mm and 50.4 mm, respectively, and $p_0$ becomes more than $154\,\mathrm{MW/m^2}$ at the EC resonant position. The value of $p_V$ is more than $95\,\mathrm{kW/m^3}$, where $V$ of $\rho \leq 0.4$ is approximately $4.1\,\mathrm{m^3}$. Therefore, this antenna system can achieve a much smaller beam width than the plasma minor radius $a \approx 0.6\,\mathrm{m}$ and enough values of $p_0$ and $p_V$ to initiate plasma in the LHD.

## 3. Investigation of dependences of plasma initiation on polarizatoin state and ECH power

The polarization of ECH is an important factor of efficient plasma heating. In the LHD, the optimum polarization setting for plasma heating is determined depending on the magnetic shear and the electron density in the peripheral region to couple the microwave beam to the intended mode [17]. The polarization state of $(\alpha, \beta) = (-45°, 0°)$ is the normally optimum setting for the X2 mode heating when the EC beam is injected perpendicularly to the toroidal direction. The oscillating electric field of the X-mode wave is perpendicular to the

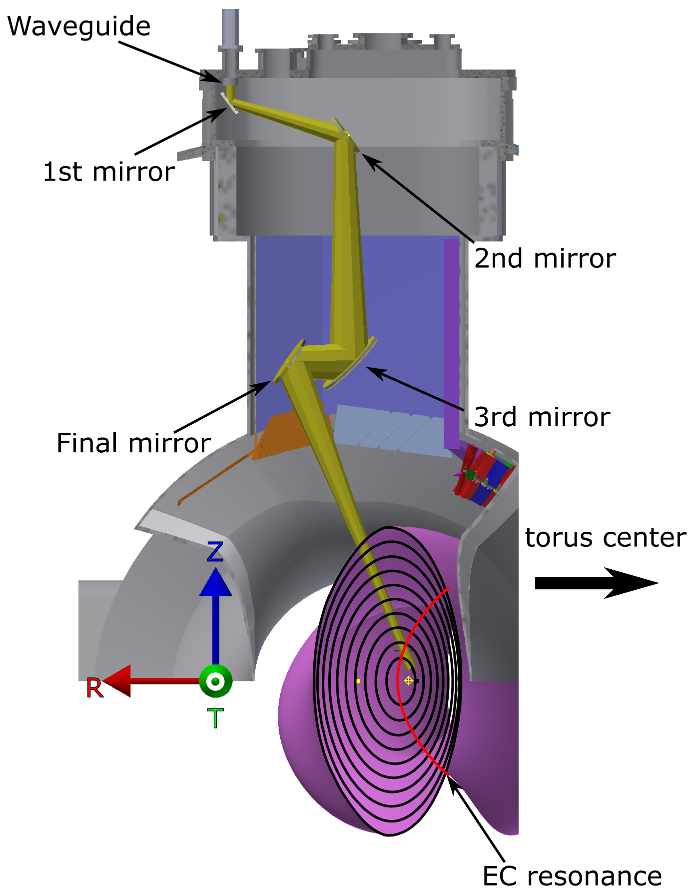


Fig. 4: Schematic view of the antenna mirrors setting and the 56 GHz Gaussian beam propagation injected into $(R, T, Z) = (3.55\,\mathrm{m}, 0\,\mathrm{m}, 0\,\mathrm{m})$ in the LHD.

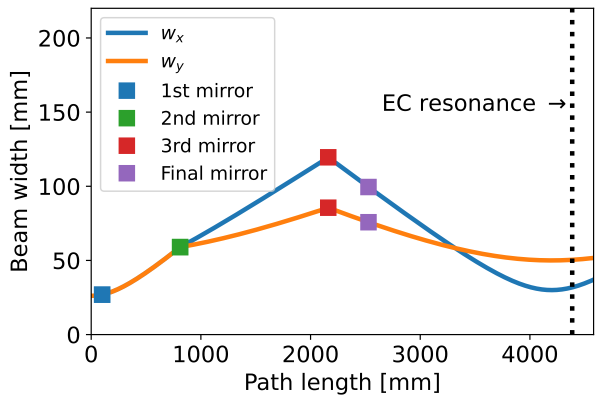


Fig. 5: Spatial evolution of the width of the 56 GHz beam injected into $(R, T, Z) = (3.55\,\mathrm{m}, 0\,\mathrm{m}, 0\,\mathrm{m})$. $w_x$ and $w_y$ are the beam width of the elliptic Gaussian beam. Each colored square indicates mirror positions along the beam path. The dotted line indicates the EC resonance position in the LHD of $(R_{ax}, B_t) = (3.6\,\mathrm{m}, 1\,\mathrm{T})$.

magnetic field and $\alpha = 90°$ and $\alpha = -90°$ are the same polarization state. The polarization around $(\alpha, \beta) = (90°, 0°)$ was the most efficient in plasma initiation by using the second harmonic EC wave in Heliotron E and Heliotron J because the injected wave was coupled well to the X2 mode at the magnetic axis[18, 19]. We experimented to investigate the effect of the polarization state on plasma startup by using the new antenna system. Note that we injected the ECH aiming to $R = 3.58\,\mathrm{m}$ on the equatorial plane in the standard magnetic configuration of $R_{ax} = 3.6\,\mathrm{m}$ and $B_t = 1\,\mathrm{T}$, where the aiming position corresponded to $\rho \approx 0.2$, in the following experiments. Figure 6 indicates the time evolution of $P_{\mathrm{ECH}}$, the neutral gas pressure $P_{cc}$ measured by a cold cathode ionization gauge, $H_\alpha$ signal, the line averaged electron density $\overline{n_e}$, and the plasma stored energy $W_p$ calculated by diamagnetic flux measurement of three polarization settings. Clear differences of plasma initiation were observed depending on the polarization while $P_{\mathrm{ECH}}$ was fixed at 390 kW. Figure 7 shows the relation between the polarization purity $\eta$ and the time delay of $H_\alpha$ and $\overline{n_e}$ reaching the target values of 0.01 and $0.2 \times 10^{18}\,\mathrm{m}^{-3}$, respectively, from the start of the ECH injection. Here, $\eta$ is expressed as follows,

$$\eta = \cos^2(\alpha - \alpha_{target})\cos^2(\beta - \beta_{target}) + \sin^2(\alpha - \alpha_{target})\sin^2(\beta + \beta_{target}),$$

$$(\alpha_{target}, \beta_{target}) = (90°, 0°).$$

Blue, green, and orange lines in Fig. 6 correspond to $\eta \approx 0.62$, 0.01, and 0.99, respectively. The time delays got shorter as $\eta$ approached unity and no plasma startup was observed less than $\eta = 0.4$. Both time delays were scattered around $\eta = 0.9$ probably because this experiment was conducted in the initial phase of the experimental campaign and the wall condition was not good. The polarization state of $(\alpha, \beta) = (90°, 0°)$ was optimum for plasma initiation because the injected wave reaches the resonant position keeping the same polarization in the vacuum of space while the mode coupling in plasma edge needs to be taken into account for plasma heating. Therefore, the optimum polarization state of plasma initiation should be different from that of plasma heating in the LHD. We confirmed that the polarization setting coupling the EC beam to the X2 mode at the magnetic axis through the vacuum of space was optimum for plasma startup in the LHD. This result was the same as Heliotron E and Heliotron J [18, 19].

Figure 8 indicates the ECH power dependence of the time delay of $H_\alpha$ and $\overline{n_e}$ reaching the same target values as Fig. 7. The polarization setting was fixed at $(\alpha, \beta) \approx (90°, 0°)$. The time delays got shorter as $P_{\mathrm{ECH}}$ increased. The data of the time delay of $H_\alpha$ when $P_{cc}$ before the ECH injection was $1 \times 10^{-4}$ Pa or less are not shown in the top panel of Fig. 8 because the time delay of $H_\alpha$ became much longer or the $H_\alpha$ signal did not even reach 0.01. The stable plasma startup was achieved by injecting the power no less than 250 kW, whose $p_0$ was more than 97 MW/m$^2$ at the EC resonance and $p_V$ was more than 108 kW/m$^3$, where $V$ of $\rho \leq 0.3$ was approximately 2.3 m$^3$. We did not observe $H_\alpha$ or $\overline{n_e}$ reaching the target value by injecting the ECH of $P_{ECH} \approx 190\,kW$ for approximately 0.23 s when $R_{ax}$ was 3.6 m. On the other hand, we confirmed the plasma initiation by the same power injection in the case of $R_{ax} = 3.55$ m.

## 4. Plasma sustainment by D-NBI with 56 GHz ECH plasma initiation

We carried out the experiment to confirm that the D-NBIs can sustain the plasma in the LHD with the help of the 56 GHz ECH system. The magnetic configuration and the injected EC beam direction were the same as the experiments in section 3. Figure 9 indicates the time evolution of $P_{\mathrm{ECH}}$ of 56 GHz and the NBI power $P_{\mathrm{NBI}}$ of #3, $P_{cc}$, $H_\alpha$, $\overline{n_e}$, the electron temperature $T_e$ at $R = 3.675$ m measured by Thomson scattering system[20], and $W_p$. $P_{\mathrm{ECH}}$ was approximately 380 kW and the polarization setting was $(\alpha, \beta) \approx (90°, 0°)$. By injecting the ECH, plasma was generated with the increase of $\overline{n_e}$, $T_e$, and $W_p$ and the plasma was sustained only by NBI#3. $\overline{n_e}$ was much higher than that of Fig. 6 because the neutral gas pressure in the vacuum vessel was moderately increased by the gas flowing from the tangential NBI systems. The value of $T_e$ can have a large margin of error in the initial phase of ECH since the electron velocity distribution can be non-Maxwellian. Plasma initiation was not observed without the ECH injection.

Figure 10 shows the time evolution of the plasma startup and sustainment with the ECH of $P_{\mathrm{ECH}} \approx 360$ kW and all NBIs of the deuterium operation. The neutral gas pressure before the ECH injection was approximately five times higher than the single NBI case indicated in Fig. 9 due to a large amount of gas flowing from perpendicular NBI systems of #4 and #5. For this reason, initiating plasma was more difficult. The increase of $\overline{n_e}$ was slower and the increase of $T_e$ and $W_p$ was not clearly observed during the injection of only the 56 GHz ECH with the polarization setting of $(\alpha, \beta) \approx (90°, 0°)$. Despite such bad condition, initiating and sustaining plasma were succeeded by using the

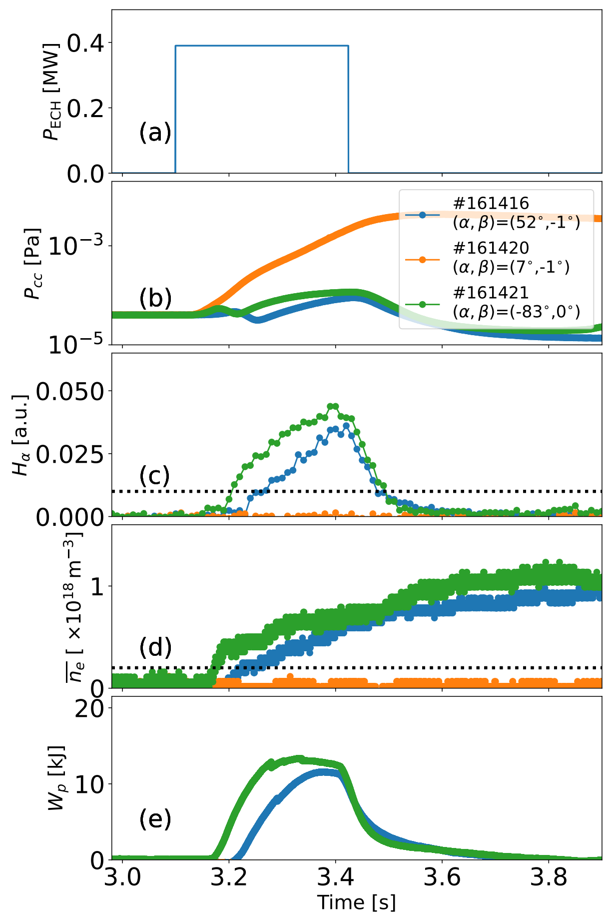


Fig. 6: Time evolution of (a) $P_{\rm ECH}$ of 56 GHz, (b) $P_{cc}$, (c) $H_\alpha$ signal, (d) $\overline{n_e}$, and (e) $W_p$. Each color indicates different polarization states $(\alpha, \beta)$ in (b), (c), (d), and (e). Dotted lines in (c) and (d) show $H_\alpha = 0.01$ and $\overline{n_e} = 0.2 \times 10^{18}\,\mathrm{m}^3$, respectively. The ECH was injected into $\rho \approx 0.2$.

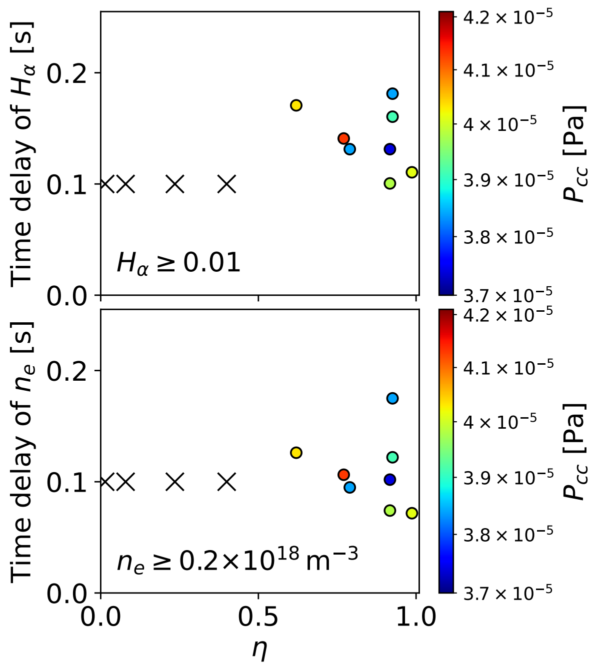


Fig. 7: Time delays of arriving at (top) $H_\alpha = 0.01$ and (bottom) $\overline{n_e} = 0.2 \times 10^{18}\,\mathrm{m}^{-3}$ from the ECH injection depending on the polarization purity of $(\alpha_{target}, \beta_{target}) = (90^\circ, 0^\circ)$. The ECH was injected into $\rho \approx 0.2$ and the power was fixed at 390 kW. The colors of circles show $P_{cc}$ before the ECH injection and it ranged from $3.7 \times 10^{-5}$ Pa to $4.2 \times 10^{-5}$ Pa. The cross marks indicate the experimented condition failing in plasma startup.

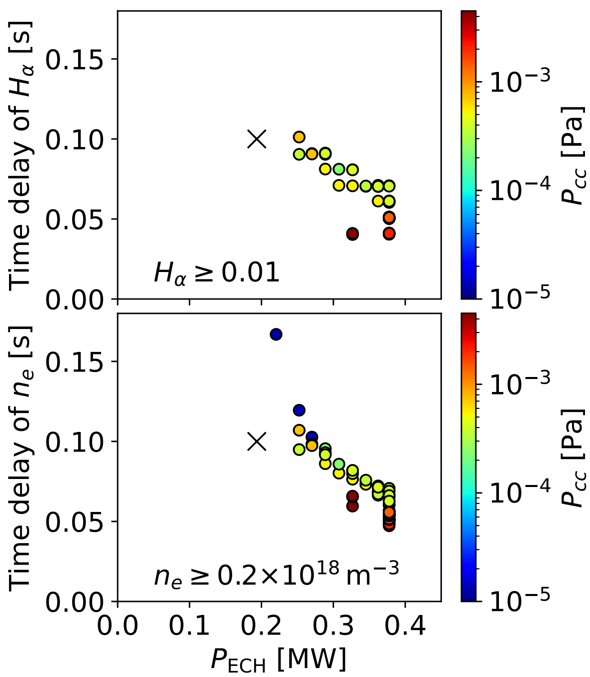


Fig. 8: Time delays of arriving at (top) $H_\alpha = 0.01$ and (bottom) $\overline{n_e} = 0.2 \times 10^{18}\,\mathrm{m}^{-3}$ from the ECH injection depending on the injected ECH power. The ECH was injected into $\rho \approx 0.2$. The colors of circles show $P_{cc}$ before the ECH injection and it ranged from $1.2 \times 10^{-5}$ Pa to $4.4 \times 10^{-3}$ Pa. The data of $P_{cc} \leq 1 \times 10^{-4}$ Pa are not shown in the top panel. The cross mark indicates the experimented condition failing in plasma startup.

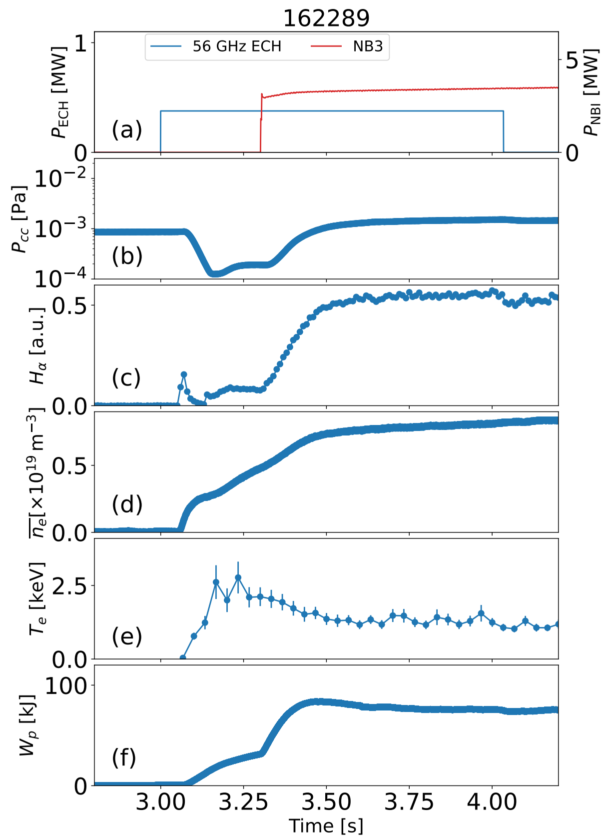


Fig. 9: Time evolution of (a) $P_{\mathrm{ECH}}$ and $P_{\mathrm{NBI}}$, (b) $P_{cc}$, (c) $H_\alpha$, (d) $\overline{n_e}$, (e) $T_e$, and (f) $W_p$.

three tangential NBIs while no plasma startup was observed without the ECH or with the ECH of $(\alpha, \beta) \approx (-45°, 0°)$.

We confirmed that the new ECH system was essential for pure deuterium plasma around $B_t = 1\,\mathrm{T}$ from these experimental results.

## 5. Summary

We constructed the 56 GHz ECH system by installing the new gyrotron, the transmission line with the polarizers, and the focusing antenna mirrors to realize high $\beta$ plasma in pure deuterium condition in the LHD. We investigated the dependences of the plasma startup on the polarization setting and the injected power of the ECH. The optimum polarization state for plasma initiation by using second harmonic EC resonance was different from that of plasma heating. We obtained the knowledge that controlling the polarization of the EC beam is needed to initiate and heat plasma more efficiently. We succeeded in initiating and sustaining plasma in the relatively low magnetic field by the tangential

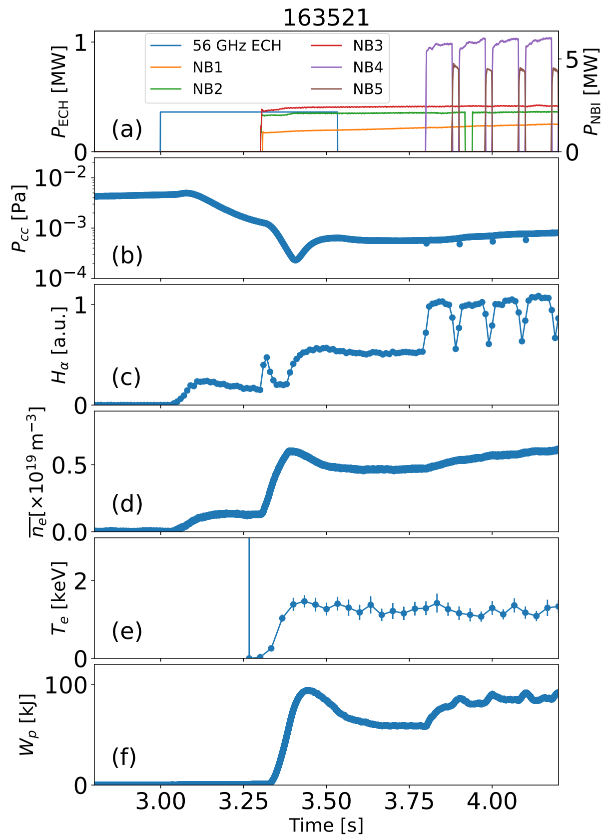


Fig. 10: Same as Fig. 9 except for injecting deuterium neutral beams by using all NBI systems.

D-NBIs with the help of the new ECH. This new ECH system contributed to expanding the regime of plasma experiments in the LHD.

## Acknowledgment

The authors are grateful to Dr. Y. Suzuki for coordinating our experiment. The authors gratefully acknowledge Prof. K. Nagasaki for his useful advice on the experiment. The authors also thank the LHD Experiment Group for the operation of the LHD.

## References

[1] R. Prater, Heating and current drive by electron cyclotron waves, Physics of Plasmas 11 (2004) 2349–2376.

[2] B. Lloyd, et al., ECRH-assisted start-up in ITER, Plasma Physics and Controlled Fusion 38 (1996) 1627–1643.

[3] J. Stober, et al., ECRH-assisted plasma start-up with toroidally inclined launch: multi-machine comparison and perspectives for ITER, Nuclear Fusion 51 (2011) 083031.

[4] A. Iiyoshi, et al., Overview of the Large Helical Device project, Nuclear Fusion 39 (1999) 1245–1256.

[5] O. Motojima, et al., Initial physics achievements of large helical device experiments, Physics of Plasmas 6 (1999) 1843–1850.

[6] T. Shimozuma, et al., ECRH-Related Technologies for High-Power and Steady-State Operation in LHD, Fusion Science and Technology 58 (2010) 530–538.

[7] H. Takahashi, et al., Extension of high Te regime with upgraded electron cyclotron resonance heating system in the Large Helical Device, Physics of Plasmas 21 (2014) 061506.

[8] Y. Takeiri, et al., High Performance of Neutral Beam Injectors for Extension of LHD Operational Regime, Fusion Science and Technology 58 (2010) 482–488.

[9] H. Takahashi, et al., Realization of high T i plasmas and confinement characteristics of ITB plasmas in the LHD deuterium experiments, Nuclear Fusion 58 (2018) 106028.

[10] S. Sakakibara, et al., Extension of high-beta plasma operation to low-collisionality regime, Nuclear Fusion 57 (2017) 066007.

[11] O. Kaneko, et al., Plasma Initiation by Neutral Beam Injection, Fusion Science and Technology 58 (2010) 497–503.

[12] K. Ikeda, et al., First results of deuterium beam operation on neutral beam injectors in the large helical device, AIP Conference Proceedings 2011 (2018) 060002.

[13] Preynas, M., et al., Experimental characterization of plasma start-up using ECRH in preparation of W7-X operation, EPJ Web of Conferences 87 (2015) 02005.

[14] K. Kajiwara, et al., Electron cyclotron heating assisted startup in JT-60U, Nuclear Fusion 45 (2005) 694–705.

[15] D. Farina, Nonlinear collisionless electron cyclotron interaction in the preionisation stage, Nuclear Fusion 58 (2018) 066012.

[16] T. Ii, et al., Design of polarizers for a mega-watt long-pulse millimeter-wave transmission line on the large helical device, Review of Scientific Instruments 86 (2015) 023502.

[17] T. Ii Tsujimura, et al., Real-time control of electron cyclotron wave polarization in the LHD, Fusion Engineering and Design 131 (2018) 130–134.

[18] K. Nagasaki, et al., Effects of magnetic shear on electron cyclotron resonance heating in heliotron/torsatron configurations, Physics of Plasmas 6 (1999) 556–564.

[19] K. Nagasaki, et al., Experimental study of plasma breakdown by second harmonic electron cyclotron waves in Heliotron J, Nuclear Fusion 45 (2004) 13–21.

[20] I. Yamada, et al., Recent Progress of the LHD Thomson Scattering System, Fusion Science and Technology 58 (2010) 345–351.